applied sciences

MDPI

Article

Mechanical Behavior of Low-Strength Hydraulic Lime Concrete Reinforced with Flexible Fibers under Quasi-Static and Dynamic Conditions

Ángel De La Rosa [1], Lucía Garijo [2], Vaibhav W. Masih [1] and Gonzalo Ruiz [1,*]

[1] ETSI Caminos, C. y P., Universidad de Castilla-La Mancha, Av. Camilo José Cela 2, 13071 Ciudad Real, Spain; angel.delarosa@uclm.es (Á.D.L.R.); vaibhavwillson.masih@uclm.es (V.W.M.)
[2] ETS de Ingeniería y Diseño Industrial, Universidad Politécnica de Madrid, Ronda de Valencia 3, 28012 Madrid, Spain; lucia.garijo@upm.es
* Correspondence: gonzalo.ruiz@uclm.es

Abstract: We investigate the effect of flexible fiber reinforcement on low-strength hydraulic lime concrete. This type of concrete is occasionally necessary to ensure compatibility with the substrate, particularly in the conservation and rehabilitation of historical heritage. For this purpose, we designed a matrix of hydraulic lime concrete based on a mix design method we proposed previously and added different amounts of polyvinyl alcohol fiber (volumetric contents of 0.3%, 0.6%, 0.9%, and 1.2%). We then conducted three-point bending tests on prismatic specimens with a central notch under quasi-static (displacement rate of 4×10^{-4} mm/s) and dynamic (4 mm/s) conditions, using a servo-hydraulic machine. The results indicate that, in both quasi-static and dynamic regimes, the flexural strength, the residual flexural strengths for different crack openings, and the work of fracture increase as the fiber content increases. Furthermore, transitioning from one regime to another (by increasing the strain rate or velocity) leads to a significant increase in these mechanical parameters.

Keywords: flexible fiber-reinforced hydraulic lime concrete; fracture mechanics; mix design method; quasi-static and dynamic flexural behavior

Citation: De La Rosa, Á.; Garijo, L.; Masih, V.W.; Ruiz, G. Mechanical Behavior of Low-Strength Hydraulic Lime Concrete Reinforced with Flexible Fibers under Quasi-Static and Dynamic Conditions. *Appl. Sci.* **2024**, *14*, 6364. https://doi.org/10.3390/app14146364

Academic Editors: Alan Wecker, Fabrizio Terenzio Gizzi and Ion Sandu

Received: 17 June 2024
Revised: 19 July 2024
Accepted: 19 July 2024
Published: 22 July 2024

1. Introduction

There is a growing inclination towards promoting contemporary sustainable construction. Research explores materials like earth-based concrete [1,2], hemp concrete [3], etc., particularly suited for applications where high mechanical strength is not essential. For instance, hemp concrete demonstrates strengths ranging from 0.1 to 1.6 MPa after 28 days. Notably, a material gaining special relevance in this context is natural hydraulic lime, despite having mechanical properties below those of Portland cement. It offers distinct advantages, primarily cost-effectiveness and reduced environmental impact, as supported by recent studies [4]. This trend extends to hydraulic lime concretes for similar reasons.

Furthermore, lime-based materials are especially suitable for the restoration of masonry buildings. In this sense, these mortars must fulfill compatibility and serviceability criteria, thus the importance of their detailed characterization [5]. With this respect, several papers focus on searching for compatible mortars to restore various structures, such as the case of the work by Moropoulou et al. [5] centered on the earthquake protection of the Kaisarini Monastery in Greece; or the work by Maravelaki-Kalaitzaki et al. [6] focused on the characterization of original mortars from a Venetian Villa in Chania, Crete; or the case of Moropoulou et al. [7], who deal with the characterization of the crushed brick/lime mortars of Justinian's Hagia Sophia to resist earthquake stresses. Recently, in 2022, Groot et al. [8] wrote the RILEM TC 277-LHS report on lime-based mortars for restoration, where they define the theoretical background and experimental developments plus positive and negative practical experiences in lime-based binders and mortars.

These lime mortars, as also happens with lime concretes, present an inherent fragility common to most cementitious materials. To counterbalance this drawback, incorporating fibers becomes crucial to enhance energy absorption capacity and ductility under various quasi-static and dynamic solicitations. This requirement has generated considerable interest in research [9].

While there is abundant scientific literature addressing the influence of different fiber types on the mechanical behavior of Portland cement concrete, the same cannot be said for natural hydraulic lime concretes. Existing studies are exclusively focused on lime mortars. Let us delve into some of the most noteworthy studies. Angiolilli et al. [10] conducted a study on hydraulic lime mortars reinforced with varying amounts and lengths of fiberglass. They observed a significant increase in the mechanical properties of the composite in quasi-static conditions, proportional to the fiber content. Notably, there was a substantial increase in fracture energy, followed by flexural strength, tensile strength, and compressive strength, in that order. This study suggests that fiberglass-reinforced lime mortar could be a viable alternative for the restoration and strengthening of historical structures [10].

Asprone et al. [4] investigated hydraulic lime mortars reinforced with basalt fibers in both quasi-static and dynamic regimes. The inclusion of fibers led to an increase in porosity, resulting in lower quasi-static compressive and flexural strengths as the fiber content increased. However, the reinforced mortars exhibited a more ductile and tough behavior. In the dynamic regime, direct tensile strength increased, showing high sensitivity to deformation velocity. Fracture energy also increased with the loading rate [4]. They concluded that basalt fiber-reinforced natural hydraulic lime mortars present good dynamic mechanical properties and may be a viable binder material for the recovery of cultural heritage. Santarelli et al. [11] studied hydraulic lime mortars reinforced with basalt fibers and different types of aggregates, showing improvements in post-cracking behavior and compressive strength, largely dependent on the matrix and basalt fiber type. They highlighted that the fibers could be surface-treated, and their content could be optimized to define a suitable material for restoration.

Badagliacco et al. [9] investigated the flexural behavior of natural hydraulic lime mortars reinforced with natural cane fibers for brick manufacturing and use in sustainable construction. Results indicated improvements in post-cracking flexural strength compared to unreinforced mortars, along with increased ductility.

Chan et al. [12] examined quasi-static responses to compression, shear, and flexure of hydraulic lime mortars reinforced with polypropylene microfibers, noting improvements in flexural toughness but increased weakness in mode I fracture. The same authors [13] also analyzed the dynamic response to impact loading in flexure, finding higher sensitivity in the lime mortar reinforced with fibers compared to Portland cement mortar and concrete reinforced with fibers. The main application of said mortars was to repair stone masonry structures of historical importance in Canada subjected to varying degrees of seismicity.

Islam et al. [14] investigated the mechanical behavior in quasi-static and dynamic regimes of hydraulic lime mortars reinforced with polypropylene microfibers in various quantities. They explained the improvement in quasi-static flexural strength and toughness with increasing fiber content, highlighting the material's sensitivity to the deformation velocity in dynamic flexural testing. Recently, Mercuri et al. [15] studied lime mortars reinforced with polyvinyl alcohol (PVA) fibers, analyzing their behavior in flexure, compression, and indirect tensile strength. The findings showed that both flexural strength and fracture energy increased with fiber content, as did tensile and compressive strengths, but at different rates. They concluded that the newly proposed mortar presented appropriate properties for the strengthening of masonry structures, especially for intervention in cultural heritage buildings.

The research on lime concretes is limited, as stated above. A chapter called "Lime Concretes with Ad Hoc Performances" authored by Rosell and Bosch can be found in the book "Building Engineering Facing the Challenges of the 21st Century" [16]. In this work, the authors use "limecrete" to refer to lime concretes and present several cases involving

the design of mortars and concretes for restoration works and new buildings. Additionally, Rosell et al. [17] designed hydraulic lime concretes to restore the Roselló church in Lérida, Spain. Besides these works, there are several papers focused on adding lime to different concretes [18–23]. However, these are not specifically designed for restoration purposes but rather for the benefits of using lime due to sustainability and economic reasons. The findings on fiber-reinforced lime concrete are extremely scant despite the potential advantages, such as increased ductility and toughness.

Furthermore, for specific applications related to both the conservation and rehabilitation of historical heritage, as well as its use in new construction, achieving compatibility requirements may not align with the desire for high compressive strength (typically defined as 6–7 MPa) [8]. Consequently, it becomes necessary to analyze the dynamic fracture behavior of this type of low-strength concrete [24–26] as opposed to that of higher-strength natural hydraulic lime concretes, whose application field is not as focused on heritage restoration and conservation. Therefore, building upon this scientific literature, this paper aims to investigate the behavior of low-strength hydraulic lime concrete reinforced with polyvinyl alcohol fibers under various loading conditions. The hydraulic lime concrete matrix was designed using an innovative methodology recently developed by the authors of this work [27]. A systematic experimental investigation was devised to examine the mode I fracture in prismatic notched beams, loaded in a three-point bending configuration at two loading velocities, covering a range of five orders of magnitude, encompassing quasi-static to dynamic regimes.

After this introduction, the paper is organized as follows. Section 2 describes the methods and materials; in Section 3, the results are presented along with a discussion. Finally, the main conclusions are provided in Section 4.

2. Materials and Methods

2.1. Mix Design Methodology

The methodology employed for formulating both the fiber-reinforced hydraulic lime concrete and its unreinforced matrix is the one presented by Garijo et al. [27]. This methodology is based on rheological and mechanical principles, encompassing the assessment of deformability in the fresh state, compressive strength, and the optimal compactness of the granular skeleton. Key design parameters include consistency in the Abrams cone, water-to-lime (w/ℓ) and superplasticizer-to-lime (SP/ℓ) relationships, and the inherent characteristics of the granular skeleton.

2.2. Materials, Manufacturing, and Characterization Methodologies

2.2.1. Raw Materials

The raw materials used in the production of flexible fiber hydraulic lime concrete (FFLC) are outlined as follows. Table 1 includes the compositions of the mix designs.

- Natural hydraulic lime NHL-3.5, ℓ (ρ_ℓ = 2580 kg/m^3).
- Local tap water, w (ρ_w = 1000 kg/m^3).
- Poli-aril-ether type-based superplasticizer, MasterEase 5025 ©, SP (ρ_{SP} = 1058 kg/m^3, dry residue = 20%).
- Rounded siliceous fine aggregate from a fluvial source FA (d_{90} = 2 mm, d_{50} = 0.87 mm, d_{10} = 0.25 mm, ρ_{FA} = 2490 kg/m^3).
- Crushed limestone coarse aggregate CA (d_{90} = 8 mm, d_{50} = 5.91 mm, d_{10} = 4 mm, ρ_{CA} = 2630 kg/m^3).
- Polyvinyl alcohol fiber, MasterFiber 400 ©, f (ℓ_f = 18 mm, d_f = 0.20 mm, λ = 90, ρ_f = 1300 kg/m^3, water absorption = 17.5%).

The mix design compositions of the hydraulic lime concrete (with and without PVA fibers) are presented in Table 1. Figure 1a plots the particle size distribution of aggregates and Figure 1b shows the morphology of the polyvinyl alcohol fibers. The use of a superplasticizer admixture is due to the interest in designing concretes (with and with-

out fiber reinforcement) within a soft consistency typology S2 (Abram's cone slump of 50–90 mm ± 10 mm) suitable for good workability with the inclusion of flexible PVA fibers. Specifically, this poly-aryl-ether type-based superplasticizer was used based on rheological tests conducted on lime pastes to determine the compatibility of the lime–superplasticizer system and the appropriate dosage ranges to achieve the desired consistency [28].

Table 1. Mix design composition of FFLC (kg of raw materials in a cubic meter of hydraulic-lime concrete).

Name	w/ℓ	SP/ℓ	Raw Materials [kg/m^3]					
			ℓ	w	SP	FA	CA	f (ϕ_f)
FFLC-0.0		0			0			0 (0%)
FFLC-0.3		0.0017			0.571			4.0 (0.3%)
FFLC-0.6	0.8	0.0033	343.2	274.6	1.143	972.0	597.0	8.0 (0.6%)
FFLC-0.9		0.0033			1.143			12.0 (0.9%)
FFLC-1.2		0.0065			2.215			16.0 (1.2%)

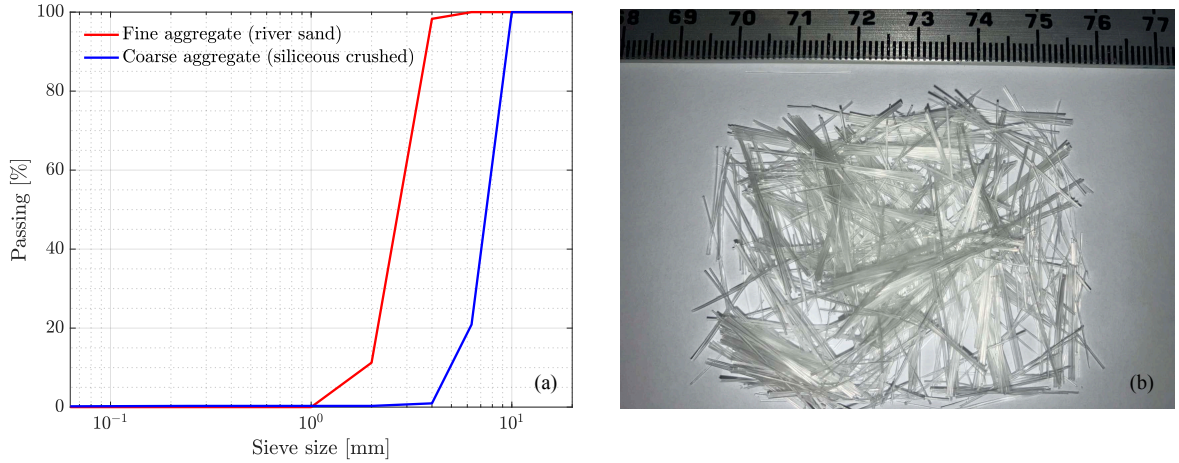

Figure 1. (**a**) Particle size distribution of aggregates; (**b**) polyvinyl alcohol fibers.

2.2.2. Manufacturing Process

The laboratory-manufactured batches were processed using a vertical-axis planetary concrete mixer with a capacity of 100 liters, handling 63 liters per batch. The concrete mixing procedure involved sequential steps: initially, dry mixing of hydraulic lime and fine aggregate for one minute, subsequent addition of 90% water over one minute, followed by an additional minute of mortar phase mixing. The superplasticizer admixture and the remaining water were then introduced for one minute, with an additional minute of mortar mixing. Subsequently, the mixing operation was briefly halted to clear material adhering to the mixer's bottom and blades. Coarse aggregate inclusion followed, with an additional two minutes of concrete mixing. Finally, the introduction of PVA fibers (in concretes with fibers) took place over one minute. The entire mixing process continued for three more minutes, concluding with the fresh state characterization of the concrete. This mixing sequence adapts our established protocol for producing Portland cement concrete [27,29]. In particular, the mixing times established in each phase have been determined and optimized based on initial tests and studies conducted in our laboratory.

Post-mixing, the concrete was poured into two types of steel molds: cylindrical specimens measuring 150 × 300 mm^2 (diameter × height) and prismatic specimens measuring 420 × 100 × 100 mm^3 (length × width × height). After casting, the specimens were stored in a room for 24 h. Subsequently, they were demolded and placed in a climatic chamber with constant temperature and humidity conditions (20 °C ± 0.5 °C, and 98% ± 0.5%, respectively) until the designated testing age. The testing age was 28 days for quasi-static characterization of compressive strength and elastic modulus, and 156 days for another

quasi-static characterization of compressive strength concurrent with dynamic fracture tests. Please note that the improvement of mechanical properties over time in NHL 3.5 is slower than in higher classes. Therefore, we decided to conduct the tests at 156 days, approximately 5 months. This time frame represents a point at which the rate of strength development becomes significantly low [8]. One week before testing, a notch, reaching a depth of 1/6 the height of the specimen, was created at the center of prismatic specimens for hydraulic lime concrete both with and without fiber reinforcement.

2.2.3. Fresh State Measurements and Quasi-Static Mechanical Characterization

In the fresh stage, a slump flow test using the Abrams cone was conducted to assess the slump characteristics of the fresh concrete batches [30]. Concurrently, the density of the fresh concrete was determined according to the guidelines outlined in [31].

In the hardened state, mechanical characterization at 28 days was undertaken; the elastic modulus was measured in cylindrical specimens measuring 150×300 mm^2 (diameter $\times$ height) as per [32]. Uniaxial compressive strength was determined in identical cylindrical specimens, controlling the load at a velocity of 0.3 MPa / s [33]. These tests were executed on a Servosis servo-hydraulic machine with a load capacity of 300 kN. At the age of conducting dynamic fracture tests (156 days), quasi-static compression strength tests were also performed.

Additionally, prismatic specimens ($420 \times 100 \times 100$ mm^3, length $\times$ width $\times$ height) were manufactured for the assessment of flexural and residual flexural strengths through three-point bending tests following [34,35]. A central notch, with a depth of 1/6 of the specimen's height, was pre-cut for subsequent testing. The value of this notch depth was chosen due to the low expected values of flexural strengths so that the specimen would not suffer damage during cutting and handling. Load-point displacements were recorded using two inductive extensometers of the LVDT type (Linear Variable Differential Transducer, HBM $\pm$ 50 mm), while CMOD (Crack Mouth Opening Displacement) was not measured due to the unavailability of a dynamic clip sensor. The testing was carried out on an Instron 8805 servo-hydraulic machine with a 1 MN capacity and a 25 kN load cell, utilizing displacement control at a velocity of 0.2 mm/min. Additionally, the work of fracture of concrete without fiber reinforcement was also determined [36–39]. All these quasi-static three-point bending tests were conducted at the time of the dynamic fracture tests (156 days).

2.2.4. Dynamic Fracture Mechanics Tests

At 156 days ($\approx$ 5 months), mode I dynamic fracture tests were conducted using the servo-hydraulic machine Instron 8805, previously employed for quasi-static mechanical characterization (Figure 2). Four prismatic specimens measuring $420 \times 100 \times 100$ mm^3, each featuring a centrally sawn notch with a depth equal to 1/6 of the specimen's height, were tested for each type of hydraulic lime concrete (with and without PVA fiber reinforcement) and at two different loading rates. The selected velocities, aiming to encompass the spectrum from quasi-static to low dynamic regimes, were denoted as $v_1 = 4 \times 10^{-4}$ mm/s and $v_2 = 4$ mm/s, respectively.

Figure 2. Configuration for a three-point bending test setup.

3. Results and Discussion

3.1. Fresh State Characterization

The presentation of the characterization results for the fresh state of both hydraulic lime concretes (with and without PVA fibers) can be found in Table 2. The density could not be measured for the mix without fibers.

Table 2. Slump in the Abrams cone test and density values.

Name	Slump [mm]	Density [kg/m^3]
FFLC-0.0	65	–
FFLC-0.3	53	2132
FFLC-0.6	65	2130
FFLC-0.9	50	2146
FFLC-1.2	55	2164

In all cases, with and without fiber reinforcement, a soft consistency is obtained in the Abrams cone test (S2 class, meaning a slump within the range 50–90 mm $\pm$ 10 mm) [40], aligning with the initial mix design goal for the fresh state. The measured fresh state density values are relatively low, possibly due to a high entrapped air content, despite vibrating the concrete in all cases.

3.2. Quasi-Static Mechanical Characterization

Tables 3 and 4 include the quasi-static mechanical characterization carried out for both hydraulic lime concretes (with and without PVA fibers) at 28 and 156 days. The data is also depicted in three bar plots in Figure 3.

Table 3. Quasi-static mechanical tests characterization results: f_c, compressive strength; E, elastic modulus (mean values, standard deviation in parentheses).

Name	f_c [MPa] (28 Days)	f_c [MPa] (156 Days)	E [GPa] (28 Days)
FFLC-0.0	1.7 (0.2)	1.5 (0.1)	7.1 (1.1)
FFLC-0.3	1.8 (0.1)	1.7 (0.1)	3.9 (1.2)
FFLC-0.6	2.0 (0.1)	2.2 (0.1)	3.2 (0.8)
FFLC-0.9	2.2 (0.1)	2.2 (0.0)	4.3 (0.3)
FFLC-1.2	2.5 (0.1)	2.5 (0.1)	2.5 (0.3)

By the initially established w/ℓ ratio during the design of the base or matrix concrete, the expected compressive strength value is achieved in all cases. Table 3 reflects how the compressive strength increases as the fiber content rises (at 28 and 156 days). While the primary effect of fiber inclusion in concrete pertains to increased ductility and toughness [41], in these cases, high fiber quantities generate a confinement effect that substantially enhances compressive strength in this type of low-strength concrete. Furthermore, Table 3 and Figure 3 show that at 156 days of age, the compressive strength of the concretes approximately matches that of 28 days, confirming that the material no longer evolves in terms of its mechanical behavior. Regarding the modulus of elasticity, Table 3 and Figure 3 indicate variability in terms of its reduction as fiber is added, except for a fiber quantity of ϕ_f = 0.9%, where an increase is observed. This could result from the greater or lesser degree of matrix disintegration due to fiber addition, as well as a potential limit or optimum value beyond which the modulus undergoes a drastic reduction.

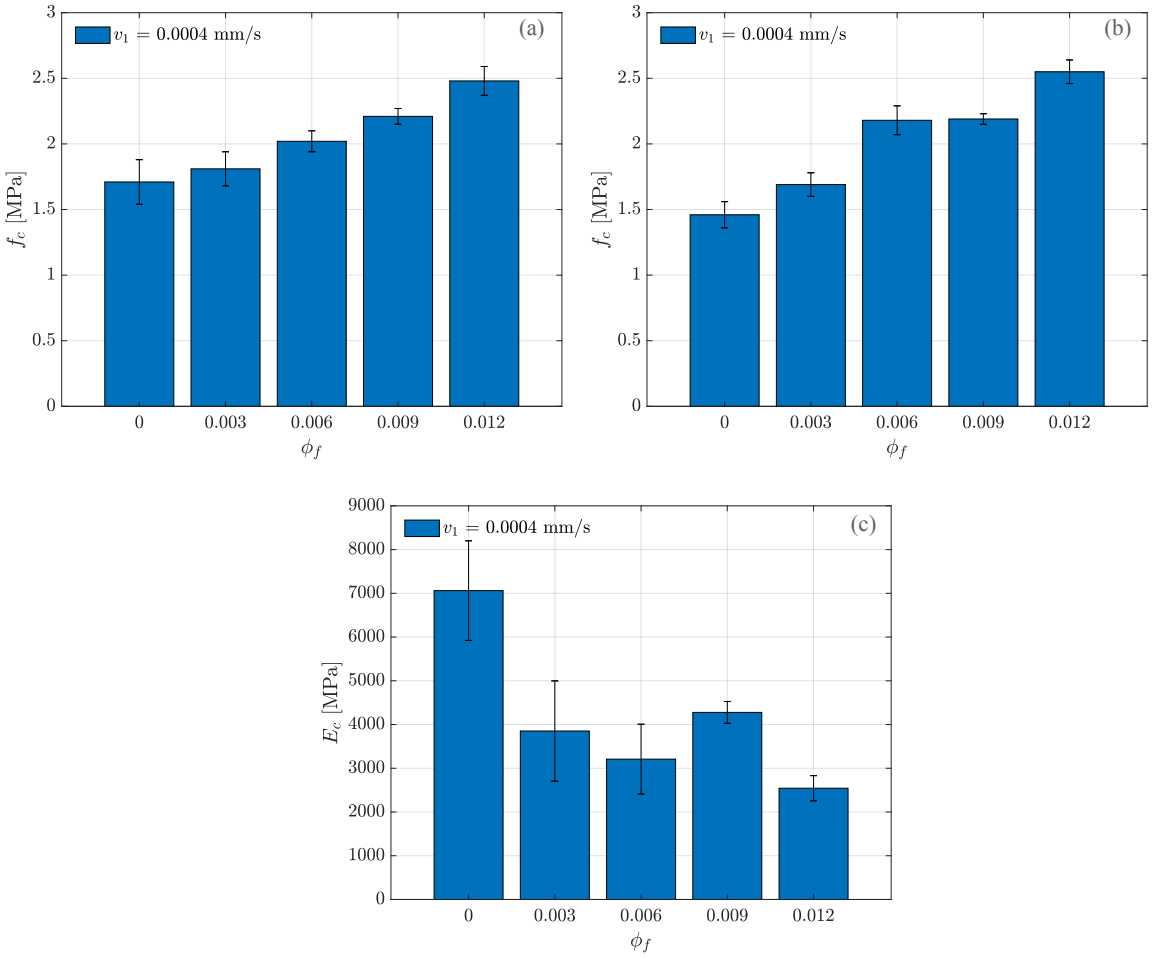

Figure 3. (**a**) f_c at 28 days, (**b**) f_c at 156 days, and (**c**) E_c at 28 days, in a quasi-static regime.

In this research, we have drawn an analogy with flexural and residual flexural strengths since, instead of being defined for crack opening values, we refer to vertical displacement values here. In other words, σ_{R1} will denote the residual flexural strength value for 0.5 mm of vertical displacement of the load application point instead of 0.5 mm of crack opening. The same procedure is followed for the remaining flexural and residual flexural strengths.

Table 4. Three point bending quasi-static tests results at a displacement rate of 0.4 µm/s (v_1): σ_N, flexural strength; σ_L, flexural strength for 0.05 mm of vertical displacement; σ_{R1}, residual flexural strength for 0.5 mm of vertical displacement; W_F, work of fracture up to 0.5 mm of vertical displacement (mean values, standard deviation in parentheses).

Name	σ_N [MPa]	σ_L [MPa]	σ_{R1} [MPa]	W_F [N m]
FFLC-0.0	0.5 (0.2)	0.2 (0.1)	–	0.14 (0.01)
FFLC-0.3	0.6 (0.2)	0.6 (0.2)	0.2 (0.1)	0.23 (0.06)
FFLC-0.6	0.6 (0.2)	0.6 (0.2)	0.4 (0.2)	0.38 (0.14)
FFLC-0.9	0.8 (0.1)	0.8 (0.1)	0.6 (0.1)	0.52 (0.07)
FFLC-1.2	0.7 (0.1)	0.7 (0.1)	0.5 (0.1)	0.48 (0.07)

3.3. Mode I Fracture Dynamic Tests

Table 5 presents a summary of mode I dynamic fracture tests conducted on hydraulic lime concretes, with and without PVA fibers, at 156 days. Additionally, graphical representations in Figures 4–7 offer a more accessible visualization of the comparative analysis and trends of various parameters.

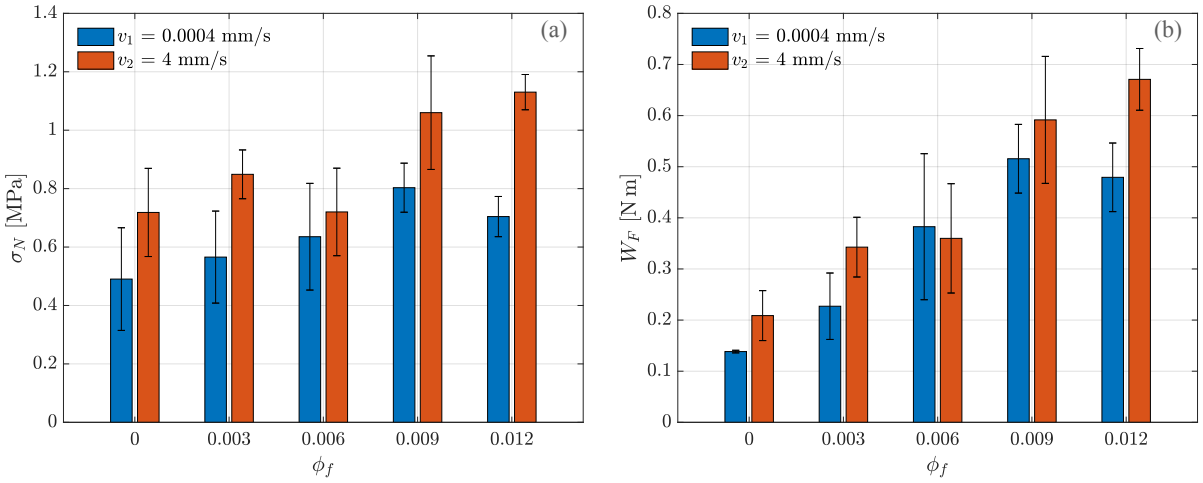

Figure 4. (**a**) σ_N and (**b**) W_F for both velocities (in notched prismatic specimens, 420 × 100 × 100 mm^3, length × height × width).

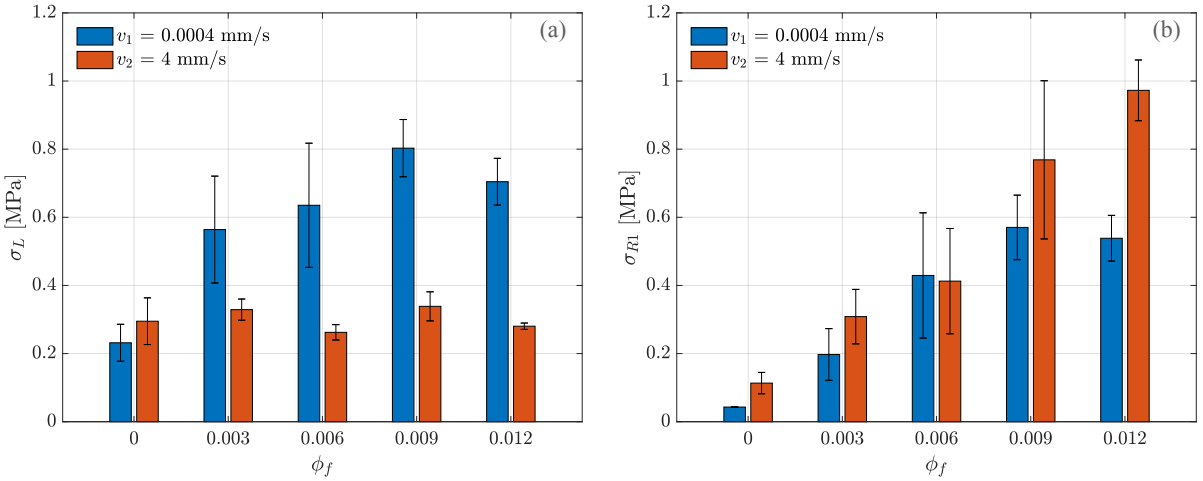

Figure 5. (**a**) σ_L and (**b**) σ_{R1} for both velocities (in notched prismatic specimens, 420 × 100 × 100 mm^3, length × height × width).

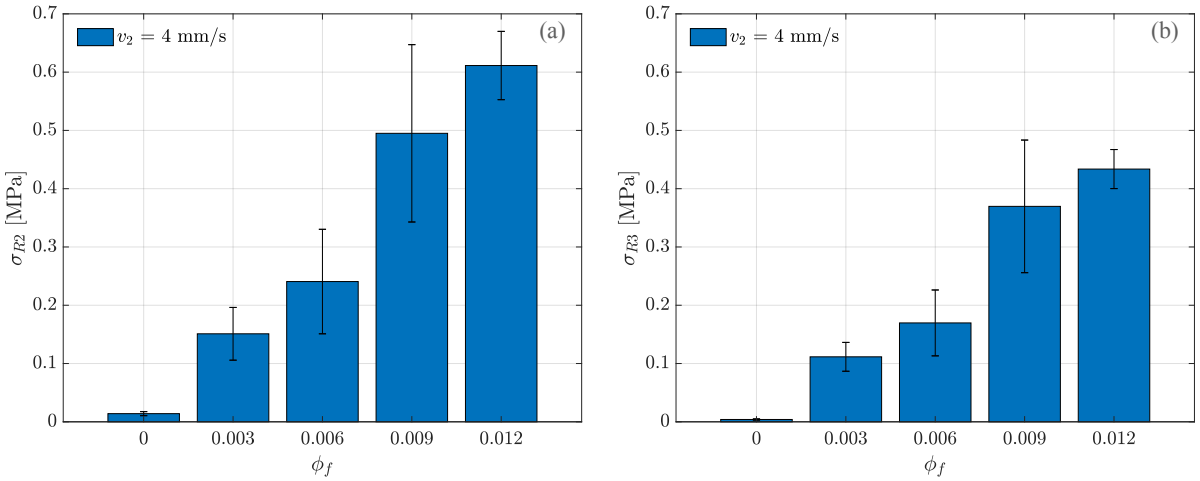

Figure 6. (**a**) σ_{R2} and (**b**) σ_{R3} for higher velocity (in notched prismatic specimens, 420 × 100 × 100 mm^3, length × height × width).

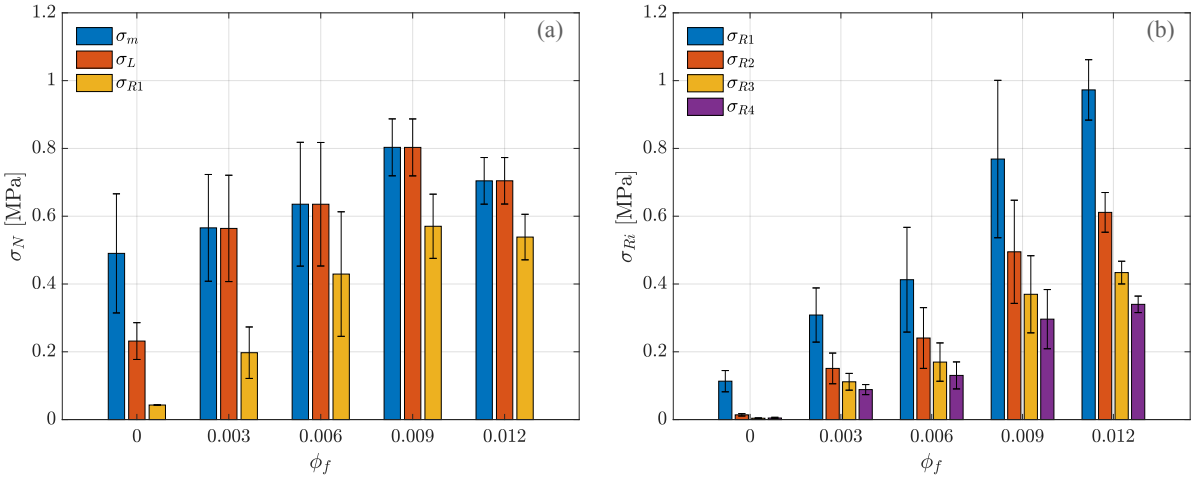

Figure 7. Evolution of flexural strengths: (**a**) σ_N (quasi-static regime); (**b**) σ_{Ri} (dynamic regime).

Table 5. Mode I fracture dynamic test results at a displacement rate of 4 mm/s (v_2): σ_N, flexural strength; σ_L, flexural strength for 0.05 mm of vertical displacement; σ_{R1}, residual flexural strength for 0.5 mm of vertical displacement; σ_{R2}, residual flexural strength for 1.5 mm of vertical displacement; σ_{R3}, residual flexural strength for 2.5 mm of vertical displacement; σ_{R4}, residual flexural strength for 3.5 mm of vertical displacement; W_F, work of fracture up to 0.5 mm of vertical displacement (mean values, standard deviation in parentheses).

Name	σ_N [MPa]	σ_L [MPa]	σ_{R1} [MPa]	σ_{R2} [MPa]	σ_{R3} [MPa]	σ_{R4} [MPa]	W_F [N m]
FFLC-0.0	0.7 (0.2)	0.3 (0.1)	0.1 (0.0)	–	–	–	0.21 (0.05)
FFLC-0.3	0.9 (0.1)	0.3 (0.0)	0.3 (0.1)	0.2 (0.1)	0.1 (0.0)	0.1 (0.0)	0.34 (0.06)
FFLC-0.6	0.7 (0.2)	0.3 (0.0)	0.4 (0.2)	0.2 (0.1)	0.2 (0.1)	0.1 (0.0)	0.36 (0.11)
FFLC-0.9	1.1 (0.2)	0.3 (0.0)	0.8 (0.2)	0.5 (0.2)	0.4 (0.1)	0.3 (0.1)	0.59 (0.12)
FFLC-1.2	1.1 (0.1)	0.3 (0.0)	1.0 (0.1)	0.6 (0.1)	0.4 (0.0)	0.3 (0.0)	0.67 (0.06)

Figure 4a compares the calculated values of σ_N under quasi-static and dynamic conditions, with loading rates $v_1 = 4 \times 10^{-4}$ mm/s and $v_2 = 4$ mm/s, respectively. In the quasi-static regime, as ϕ_f increases, so does σ_N, reaching its maximum value at $\phi_f = 0.009$. In the dynamic regime, there is likewise an increasing trend for σ_N as ϕ_f is augmented, except at $\phi_f = 0.006$, where it decreases relatively. Additionally, values of W_F have been measured at both loading rates for fiber-unreinforced concretes up to 0.5 mm of vertical

displacement under the loading point (Figure 4b). As anticipated, in the dynamic regime, the W_F value is higher than in the quasi-static regime, except for ϕ_f = 0.006 of fiber content. Given that the average W_F values are quite similar, and the standard deviation is relatively high at both speeds, the most likely explanation for this atypical trend is the lack of uniformity in the distribution and quantity of fibers crossing the fracture section.

Figure 5 compares the obtained values of σ_L and σ_{R1} for both regimes. In the quasi-static regime, as ϕ_f increases, so does σ_L, reaching the optimum value at ϕ_f = 0.009. Meanwhile, in the dynamic regime, σ_L remains constant as ϕ_f increases (Figure 5a). Regarding residual flexural strength, only the evolution of σ_{R1} can be compared since it is the only measurable parameter in both regimes (Figure 5b). In the quasi-static regime, a similar trend to σ_L is observed; as ϕ_f increases, so does σ_{R1}, reaching the optimal value again at ϕ_f = 0.009. In the dynamic regime, the value of σ_{R1} increases with the increase in ϕ_f.

Figure 6 illustrates the dynamic regime evolution of residual flexural strength values for 1.5 mm and 2.5 mm of vertical displacement, σ_{R2} and σ_{R3}, respectively. Both strength parameters are enhanced as ϕ_f is increased.

Figure 7a compares the evolution of flexural strength parameters measured in the quasi-static regime ($v_1 = 4 \times 10^{-4}$ mm/s). Except for the unreinforced matrix, σ_N and σ_L coincide for different fiber quantities. It is also observed that the values of σ_{R1} follow a similar trend to σ_N and σ_L for various ϕ_f values, reaching their maximum values at ϕ_f = 0.009. This indicates that, for the studied hydraulic lime concrete matrix design, there exists an optimal fiber volume fraction (ϕ_f = 0.009) in the quasi-static regime, beyond which distortion occurs, leading to reduced flexural strengths.

Figure 7b compares the evolution of residual flexural strength (σ_{R1}, σ_{R2}, σ_{R3}, and σ_{R4}) measured in the dynamic regime (v_2 = 4 mm/s). All parameters show an increase as the fiber volume fraction is augmented. Additionally, their growth rates remain approximately constant across the entire ϕ_f range.

Figures 8a,b depict the stress–displacement curves, σ-δ, for three-point bending tests under quasi-static and dynamic conditions, respectively. In the quasi-static regime (Figure 8a), specimen failure occurs at displacements, δ, around 0.5 mm for fiber-unreinforced concretes and approximately 1 mm for fiber-reinforced concretes. An increase in flexural energy absorption capacity is also evident as ϕ_f is augmented. In the dynamic regime (Figure 8b), all fiber-reinforced concretes exhibit residual flexural strength values for displacements of at least 3.5 mm. Furthermore, the flexural energy absorption capacity not only increases with fiber content but is significantly higher than that calculated in the quasi-static regime for all cases, including fiber-unreinforced concretes, as previously explained (Figure 4b).

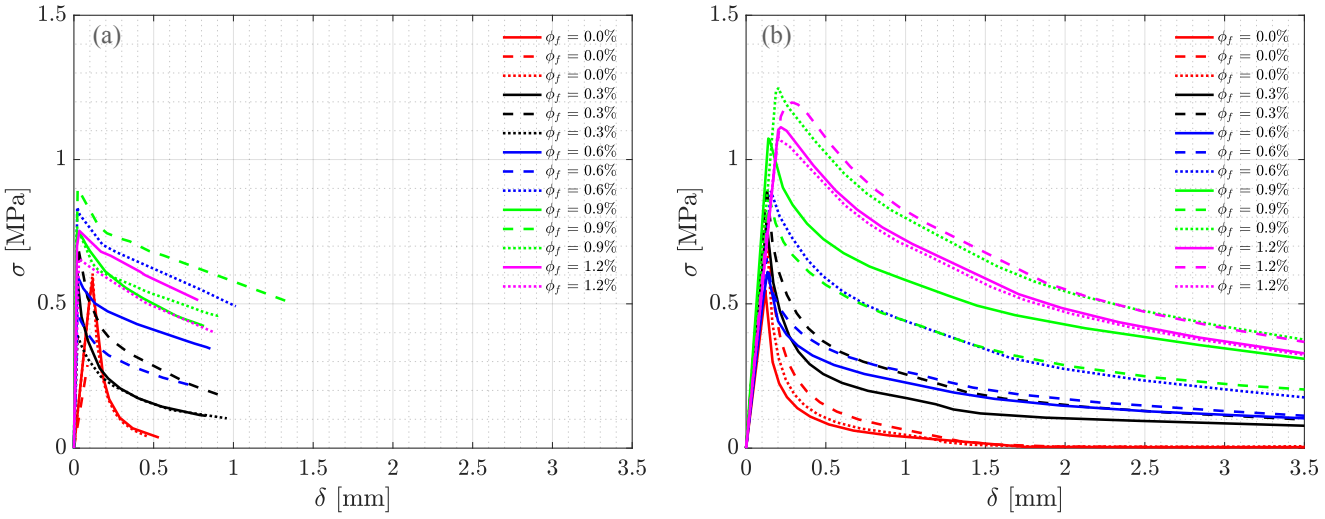

Figure 8. Three-point bending test curves: (**a**) $v_1 = 4 \times 10^{-4}$ mm/s; (**b**) v_2 = 4 mm/s.

As depicted in Figures 7 and 8, the evolution of residual flexural strengths for different vertical displacement values is noteworthy in the dynamic regime as fiber is added to hydraulic lime concrete. This highlights the effective interaction at the fiber–matrix interface, confirmed through post-mortem analysis of specimens where the predominant fiber failure is pullout. This interaction allows the composite material to develop energy absorption capacity and ductility in the post-peak load range. This translates into the suitability of discontinuous reinforcement with this fiber type in lime concretes susceptible to specific ranges of dynamic loading.

3.4. Discussion

Fiber-reinforced concrete proves highly suitable for withstanding dynamic forces owing to its heightened ductility and increased ability to dissipate energy during fractures. Over the past few decades, research has extensively addressed the initiation and progression of mode I fracture cracks in plain Portland cement concrete, employing both experimental and numerical approaches. As concrete is inherently prone to damage and fracture, the loading rate plays a pivotal role in influencing its strength, failure mode, and ultimate crack patterns [42–45]. This response may be attributed to various factors, including the growth of micro-cracks associated with loading rate, the viscous behavior influenced by water content, or the Steffan effect [46], and the impact of structural inertia forces. These forces, stemming from crack propagation, inertia activated by material hardening or softening, and inertia due to crack bifurcation, can alter the stress–strain state.

The first two factors dominate at lower loading rates, while the third becomes more significant at higher loading rates. Concrete properties, such as bending [47–49], have been demonstrated to be rate-dependent. Consequently, applying quasi-static mechanical properties to structures becomes inappropriate when dynamic effects are significant. The introduction of fibers enhances the material's toughness by improving the stitching capacity of fibers for developed cracks through the pullout mechanism [50,51]. Simultaneously, the dynamic fracture of fiber-reinforced concrete in mode I becomes more intricate. Zhang et al. [45,52] conducted a study on the dynamic fracture of fiber-reinforced concrete, shedding light on these complexities.

Therefore, characterizing these properties under dynamic loading conditions becomes imperative. In particular, the findings from this study are consistent with the existing scientific literature on Portland cement concrete. However, this work represents a relevant and novel contribution to fiber-reinforced lime concrete knowledge. Indeed, restoration and repair elements in heritage structures may need to sustain wind loads, earthquakes, cyclic loads, impacts, etc. Therefore, the reinforcement of natural hydraulic lime concrete with flexible fibers (in this case, PVA) is beneficial from multiple perspectives for use in heritage restoration and repair elements regarding strength, durability, and sustainability (economic, social, and environmental). It is noteworthy that one of the limitations identified in this study will be addressed in a subsequent article, where the results under impact loads will be analyzed. Therefore, for a proper interpretation of the findings in this study, it is crucial to bear in mind this important consideration.

Figure 9 depicts the typical cracking pattern in a three-point bending test under mode I fracture on a specimen with a central notch. Upon dynamic loading, the initial observation is the development of the primary crack extending from the notch tip towards the loading point (Figure 10). In the dynamic regime, failure occurs along the intergranular regions of the fractured surface (Figure 11). Additionally, it is noted that the fibers predominantly fail through pullout, occasionally experiencing breakage (Figure 11). These characteristics of inter-granular fracture mode and predominant fiber pullout are similar to those observed in the quasi-static regime.

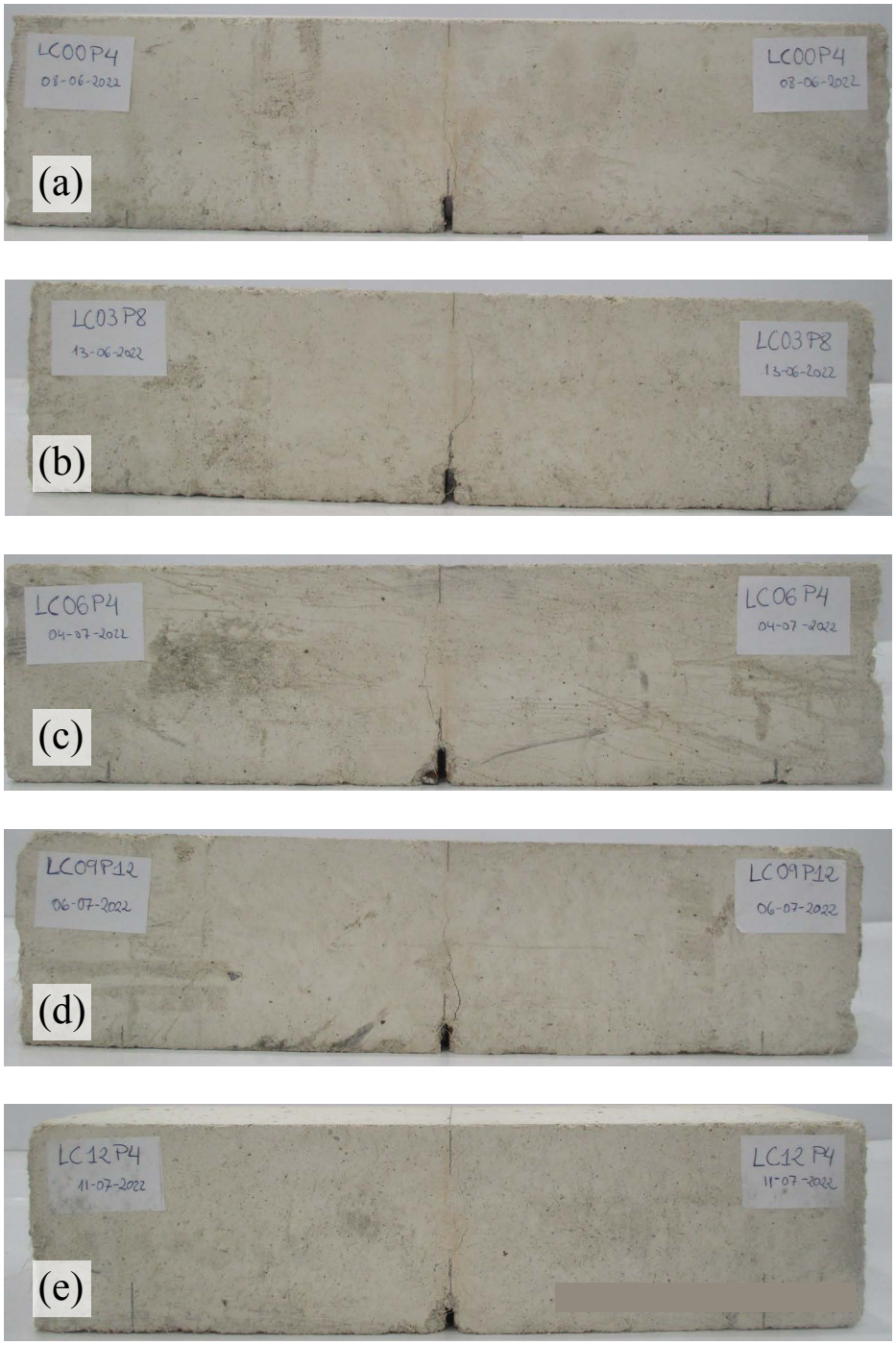

Figure 9. Typical crack patterns for quasi-static three point bending test: (**a**) ϕ_f = 0%, (**b**) ϕ_f = 0.3%, (**c**) ϕ_f = 0.6%, (**d**) ϕ_f = 0.9%, (**e**) ϕ_f = 1.2%.

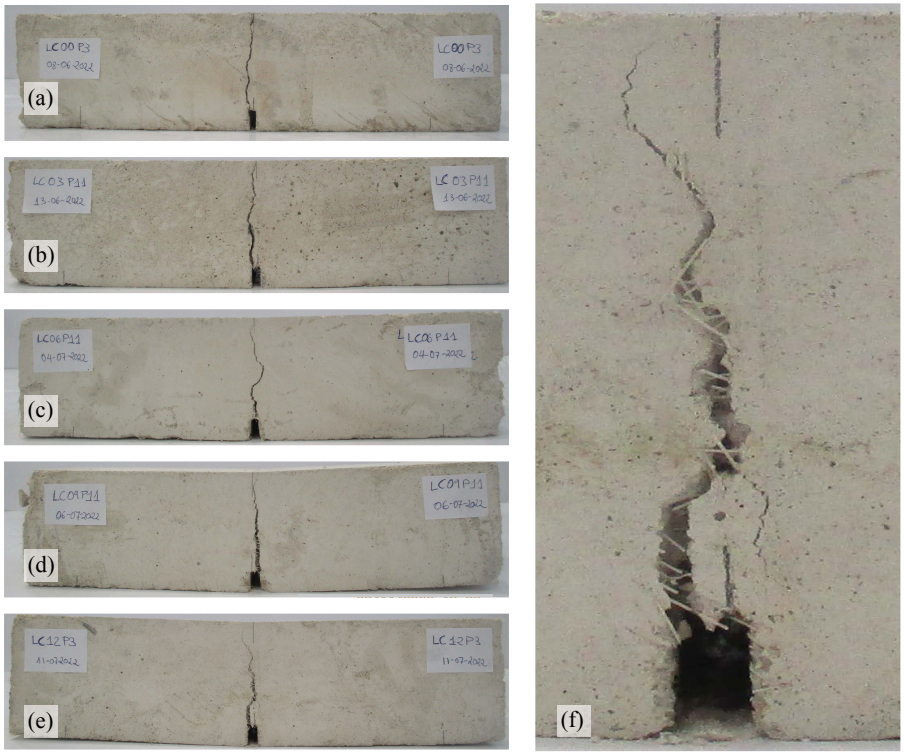

Figure 10. Crack patterns in mode I of fracture dynamic: (**a**) ϕ_f = 0%, (**b**) ϕ_f = 0.3%, (**c**) ϕ_f = 0.6%, (**d**) ϕ_f = 0.9%, (**e**) ϕ_f = 1.2%, (**f**) detail of fibers crossing the crack in hydraulic lime fiber-reinforced concrete with ϕ_f = 1.2%.

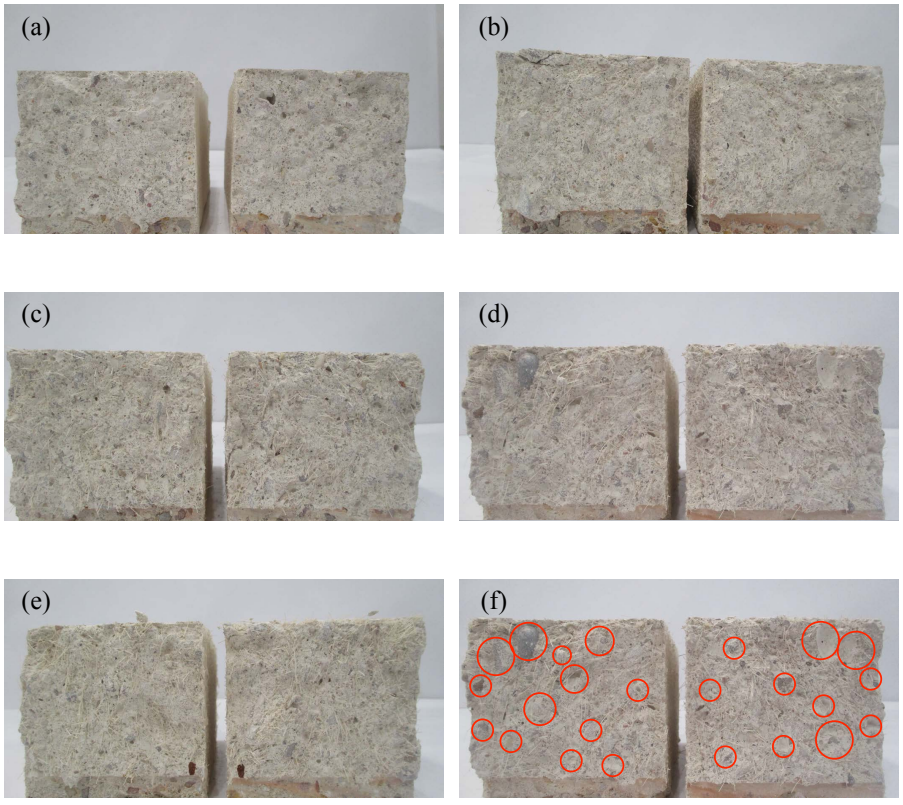

Figure 11. Perceivable inter-granular failure of fracture dynamic tests: (**a**) ϕ_f = 0%, (**b**) ϕ_f = 0.3%, (**c**) ϕ_f = 0.6%, (**d**) ϕ_f = 0.9%, (**e**) ϕ_f = 1.2%, (**f**) detail of inter-granular fracture in hydraulic lime fiber-reinforced concrete with ϕ_f = 0.9%.

4. Conclusions

In this study, we examine the effects of flexible PVA fiber reinforcement on low-strength hydraulic lime concrete under both quasi-static and dynamic conditions. The research involves prismatic specimens with varying polyvinyl alcohol fiber contents, subjected to three-point bending tests. In both hydraulic lime concretes (with and without PVA fibers), the fresh state characterization revealed a soft consistency in the Abrams cone test, aligning with the design goal. Relatively low fresh state density values were observed, possibly attributed to a high content of entrapped air.

Concerning the quasi-static mechanical characterization, the expected compressive strength value was achieved in all cases, aligned with the initially established w/ℓ ratio in the mix design. The compressive strength increased with the rise in fiber content, showcasing a substantial enhancement in low-strength concrete. The modulus of elasticity exhibited variability, generally decreasing with fiber inclusion, except for $\phi_f = 0.9\%$. An optimal fiber volume fraction ($\phi_f = 0.9\%$) was identified for maximum flexural strengths in the quasi-static regime, beyond which a reduction occurred.

Dynamic fracture tests demonstrated increased flexural strength parameters as fiber volume fraction increased. Residual flexural strengths (σ_{R1}, σ_{R2}, σ_{R3}, σ_{R4}) in the dynamic regime consistently grew with augmented ϕ_f, with constant growth rates. The stress–crack opening curves in three-point bending tests revealed enhanced energy absorption capacity and ductility in the dynamic regime, emphasizing the effectiveness of fiber–matrix interaction.

An increase in flexural strength, residual flexural strengths, and work of fracture is observed with higher fiber content in both regimes. Transitioning between regimes significantly enhances these mechanical properties. Post-mortem analysis confirmed intergranular fracture and effective fiber–matrix interaction, primarily through fiber pullout failure. This interaction facilitated the development of energy absorption capacity and ductility in the post-peak load range.

The study highlights the suitability of discontinuous PVA fiber reinforcement in lime concretes under specific dynamic loading conditions. The results offer valuable insights for optimizing fiber content to improve mechanical properties and fracture strength in lime concretes. The composite material exhibits significant ductility and energy absorption capacity, rendering it a promising alternative for various applications including restoration, rehabilitation, and new construction projects.

Author Contributions: Á.D.L.R.: Conceptualization, writing—original draft preparation and review and editing, methodology, experimental results and validation. L.G.: Conceptualization, writing—review and editing, methodology, validation. V.W.M.: Writing—review and editing, experimental results. G.R.: Conceptualization, writing—review and editing, methodology, validation, resources. All authors have read and agreed to the published version of the manuscript.

Funding: This research received funding from the Universidad de Castilla-La Mancha, Spain, jointly with the Fondo Europeo de Desarrollo Regional through grant 2022–GRIN–34124, and from the Ministerio de Ciencia e Innovación, Spain, through grants PID2019–110928RB–C31 and PID2021–124521OB–I00.

Institutional Review Board Statement: Not applicable.

Informed Consent Statement: Not applicable.

Data Availability Statement: Data will be made available on request.

Acknowledgments: The authors acknowledge the free supply of raw materials provided by Master Builders Solutions.

Conflicts of Interest: The authors declare no conflicts of interest. The funders had no role in the design of the study; in the collection, analyses, or interpretation of data; in the writing of the manuscript; or in the decision to publish the results.

References

1. Ardant, D.; Brumaud, C.; Perrot, A.; Habert, G. Robust clay binder for earth-based concrete. *Cem. Concr. Res.* **2023**, *172*, 107207. [CrossRef]
2. Keita, E.; Perrot, A. Processing of earth-based materials: Current situation and challenges ahead. *RILEM Tech. Lett.* **2023**, *8*, 141–149. [CrossRef]
3. Abdalqader, A.; Fayyad, F.; Sonebi, M.; Taylor, S. Characterisation of Hemp Shiv and its Effect on the Compressive Strength of Hemp Concrete. In Proceedings of the International RILEM Conference on Synergising Expertise towards Sustainability and Robustness of Cement-Based Materials and Concrete Structures, Milos, Greece, 14–16 June 2023; Springer: Cham, Switzerland, 2023; Volume 43, pp. 1–11. [CrossRef]
4. Asprone, D.; Cadoni, E.; Iucolano, F.; Prota, A. Analysis of the strain-rate behavior of a basalt fiber reinforced natural hydraulic mortar. *Cem. Concr. Compos.* **2014**, *53*, 52–58. [CrossRef]
5. Moropoulou, A.; Apostolopoulou, M.; Moundoulas, P.; Aggelakopoulou, E.; Siouta, L.; Bakolas, A.; Douvika, M.; Karakitsios, P.; Asteris, G. The role of restoration mortars in the earthquake protection of the Kaisariani Monastery. In Proceedings of the ECCOMAS Congress 2016, VII European Congress on Computational Methods in Applied Sciences and Engineering, Crete, Greece, 5–10 June 2016.
6. Maravelaki-Kalaitzaki, P.; Bakolas, A.; Karatasios, I.; Kilikoglou, V. Hydraulic lime mortars for the restoration of historic masonry in Crete. *Cem. Concr. Res.* **2005**, *35*, 1577–1586. [CrossRef]
7. Moropoulou, A.; Cakmak, A.; Biscontin, G.; Bakolas, A.; Zendri, E. Advanced Byzantine cement based composites resisting earthquake stresses: The crushed brickylime mortars of Justinian's Hagia Sophia. *Constr. Build. Mater.* **2002**, *16*, 543–552. [CrossRef]
8. Groot, C.; Veiga, R.; Papayianni, I.; Van Hees, R.; Secco, M.; Álvarez, J.; Faria, P.; Stefanidou, M. RILEM TC 277-LHS report: Lime-based mortars for restoration—A review on long-term durability aspects and experience from practice. *Mater. Struct.* **2022**, *55*, 245. [CrossRef]
9. Badagliacco, D.; Megna, B.; Valenza, A. Induced Modification of Flexural Toughness of Natural Hydraulic Lime Based Mortars by Addition of Giant Reed Fibers. *Case Stud. Constr. Mater.* **2020**, *13*, e00425. [CrossRef]
10. Angiolilli, M.; Gregori, A.; Vailati, M. Lime-Based Mortar Reinforced by Randomly Oriented Short Fibers for the Retrofitting of the Historical Masonry Structure. *Materials* **2020**, *13*, 3462. [CrossRef] [PubMed]
11. Santarelli, M.; Sbardella, F.; Zuena, M.; Tirillò, J.; Sarasini, F. Basalt fiber reinforced natural hydraulic lime mortars: A potential bio-based material for restoration. *Mater. Des.* **2014**, *63*, 398–406. [CrossRef]
12. Chan, R.; Bindiganavile, V. Toughness of fibre reinforced hydraulic lime mortar. Part-1: Quasi-static response. *Mater. Struct.* **2010**, *43*, 1435–1444. [CrossRef]
13. Chan, R.; Bindiganavile, V. Toughness of fibre reinforced hydraulic lime mortar. Part-2: Dynamic response. *Mater. Struct.* **2010**, *43*, 1445–1455. [CrossRef]
14. Islam, T.; Chan, R.; Bindiganavile, V. Stress rate sensitivity of stone masonry units bound with fibre reinforced hydraulic lime mortar. *Mater. Struct.* **2012**, *45*, 765–776. [CrossRef]
15. Mercuri, M.; Vailati, M.; Gregori, A. Lime-based mortar reinforced with randomly oriented polyvinyl-alcohol (PVA) fibers for strengthening historical masonry structures. *Dev. Built Environ.* **2023**, *14*, 100152. [CrossRef]
16. David Bienvenido-Huertas, J.D.Á. (Ed.) *Building Engineering Facing the Challenges of the 21st Century. Holistic Study from the Perspectives of Materials, Construction, Energy and Sustainability*; Springer: Singapore, 2023.
17. Rosell, J.; Ramírez-Casas, J.; Bedini, S.; Sala, M. Hormigón de cal para la restauración de la Iglesia del Roselló (Lérida). In Proceedings of the Construction Pathology, Rehabilitation Technology and Heritage Management (7th REHABEND Congress), Cáceres, Spain, 15–18 May 2018; Volume 134, pp. 15–18.
18. Adesina, P.A.; Olutoge, F.A. Structural properties of sustainable concrete developed using rice husk ash and hydrated lime. *J. Build. Eng.* **2019**, *25*, 100804. [CrossRef]
19. Kinnane, O.; Reilly, A.; Grimes, J.; Pavia, S.; Walker, R. Acoustic absorption of hemp-lime construction. *Constr. Build. Mater.* **2016**, *122*, 674–682. [CrossRef]
20. George, S.; Sofi, A. Enhancement of Fly Ash Concrete By Hydrated Lime and Steel Fibres. *Mater.-Today-Proc.* **2017**, *4*, 9807–9811. [CrossRef]
21. Courard, L.; Degee, H.; Darimont, A. Effects of the presence of free lime nodules into concrete: Experimentation and modelling. *Cem. Concr. Res.* **2014**, *64*, 73–88. [CrossRef]
22. Barbhuiya, S.A.; Gbagbo, J.K.; Russell, M.I.; Basheer, P.A.M. Properties of fly ash concrete modified with hydrated lime and silica fume. *Constr. Build. Mater.* **2009**, *23*, 3233–3239. [CrossRef]
23. Grist, E.R.; Paine, K.A.; Heath, A.; Norman, J.; Pinder, H. Structural and durability properties of hydraulic lime-pozzolan concretes. *Cem. Concr. Compos.* **2015**, *62*, 212–223. [CrossRef]
24. Velosa, A.; Cachim, P. Hydraulic-lime based concrete: Strength development using a pozzolanic addition and different curing conditions. *Constr. Build. Mater.* **2009**, *23*, 2107–2111. [CrossRef]
25. Rosell, J.; Bosch, M. Hormigones de cal: Nuevos "viejos" materiales. In Proceedings of the Tradición, Versatilidad e Innovación en la cal: Un Material de Excelencia VI Jornadas FICAL, Pamplona, Spain, 28–30 May 2018.

26. Malathy, R.; Shanmugam, R.; Dhamotharan, D.; Kamaraj, D.; Prabakaran, M.; Kim, J. Lime based concrete and mortar enhanced with pozzolanic materials—State of art. *Constr. Build. Mater.* **2023**, *390*, 131415. [CrossRef]
27. Garijo, L.; De La Rosa, A.; Ruiz, G. Bridging history and innovation: Advanced mix design techniques for enhanced lime concrete performance. 2024, *submitted*.
28. De La Rosa, A.; Ruiz, G.; Moreno, R. Analysis of the rheological properties of natural hydraulic lime-based suspensions for sustainable construction and heritage conservation. *Materials* **2024**, *17*, 825. [CrossRef] [PubMed]
29. De La Rosa, Á.; Poveda, E.; Ruiz, G.; Cifuentes, H. Proportioning of self-compacting steel-fiber reinforced concrete mixes based on target plastic viscosity and compressive strength: Mix-design procedure & experimental validation. *Constr. Build. Mater.* **2018**, *189*, 409–419. [CrossRef]
30. *UNE-EN-12350-2:2020*; Testing Fresh Concrete—Part 2: Slump Test. CEN–European Committee for Standardization: Brussels, Belgium, 2020.
31. *UNE-EN-12350-6:2020*; Testing Fresh Concrete—Part 6: Density. CEN—European Committee for Standardization: Brussels, Belgium, 2020.
32. *UNE-EN-12390-13:2022*; Testing Hardened Concrete—Part 13: Determination of Secant Modulus of Elasticity in Compression. CEN—European Committee for Standardization: Brussels, Belgium, 2022.
33. *UNE-EN-12390-3:2020*; Testing Hardened Concrete—Part 3: Compressive Strength of Test Specimens. CEN—European Committee for Standardization: Brussels, Belgium, 2020.
34. Vandewalle, L.; Nemegeer, D.; Balazs, L.; Barr, B.; Barros, J.; Bartos, P.; Banthia, N.; Criswell, M.; Denarie, E.; Di Prisco, M.; et al. RILEM TC 162-TDF: Test and design methods for steel fibre reinforced concrete'—Sigma-epsilon-design method—Final Recommendation. *Mater. Struct.* **2003**, *36*, 560–567. [CrossRef]
35. *UNE–EN 14651:2007+A1:2008*; Test Method for Metallic Fibre Concrete—Measuring the Flexural Tensile Strength (Limit of Proportionality (LOP), Residual). CEN—European Committee for Standardization: Brussels, Belgium, 2008.
36. Curbach, M.; Eibl, J. Determination of the fracture energy of mortar and concrete by means of the three–point bend tests on notched beams (RILEM Draft Recommendation, TC–50–FMC Fracture Mechanics of Concrete). *Mater. Struct.* **1985**, *18*, 287–290. [CrossRef]
37. Guinea, G.; Planas, J.; Elices, M. Measurement of the fracture energy using three–point bend tests: Part 1—Influence of experimental procedures. *Mater. Struct.* **1992**, *25*, 212–218. [CrossRef]
38. Planas, J.; Elices, M.; Guinea, G. Measurement of the fracture energy using three-point bend tests: Part 2—Influence of bulk energy dissipation. *Mater. Struct.* **1992**, *25*, 305–312. [CrossRef]
39. Elices, M.; Guinea, G.; Planas, J. Measurement of the fracture energy using three-point bend tests: Part 3—Influence of cutting the P–δ tail. *Mater. Struct.* **1992**, *25*, 327–334. [CrossRef]
40. *UNE-EN-206:2013+A2*; Concrete—Specification, Performance, Production and Conformity. CEN—European Committee for Standardization: Brussels, Belgium, 2021.
41. Ruiz, G.; De La Rosa, A.; Poveda, E.; Zanon, R.; Schäfer, M.; Wolf, S. Compressive Behaviour of Steel-Fibre Reinforced Concrete in Annex L of New Eurocode 2. *Hormig. Acero* **2023**, *74*, 187–198. [CrossRef]
42. Ožbolt, J.; Bošnjak, J.; Emiliano Sola, E. Dynamic fracture of concrete compact tension specimen: Experimental and numerical study. *Int. J. Solids Struct.* **2013**, *50*, 4270–4278. [CrossRef]
43. Reinhardt, H.; Weerheijm, J. Tensile fracture of concrete at high loading rates taking account of inertia and crack velocity effects. *Int. J. Fract.* **1991**, *51*, 31–42. [CrossRef]
44. Ožbolt, J.; Rah, K.; Meštrović, D. Influence of loading rate on concrete cone failure. *Int. J. Fract.* **2006**, *139*, 239–252. [CrossRef]
45. Zhang, X.; Abd Elazim, A.; Ruiz, G.; Yu, R. Fracture behaviour of steel fibre-reinforced concrete at a wide range of loading rates. *Int. J. Impact Eng.* **2014**, *71*, 89–96. [CrossRef]
46. Zheng, D.; Li, Q. An explanation for rate effect of concrete strength based on fracture toughness including free water viscosity. *Eng. Fract. Mech.* **2004**, *71*, 2319–2327. [CrossRef]
47. Banthia, N.; Mindess, S.; Bentur, A.; Pigeon, M. Impact testing of concrete using a drop-weight impact machine. *Exp. Mech.* **1989**, *29*, 63–69. [CrossRef]
48. Suaris, W.; Shah, S. Strain-rate effects in fibre-reinforced concrete subjected to impact and impulsive loading. *Composites* **1982**, *13*, 153–159. [CrossRef]
49. Gopalaratnam, V.; Shah, S.; John, R. A modified instrumented charpy test for cement-based composites. *Exp. Mech.* **1984**, *24*, 102–111. [CrossRef]
50. Yoo, D.; Banthia, N. Impact resistance of fiber-reinforced concrete—A review. *Cem. Concr. Compos.* **2019**, *104*, 103389. [CrossRef]
51. Naaman, A.; Gopalaratnam, V. Impact properties of steel fibre reinforced concrete in bending. *Int. J. Cem. Compos. Lightweight Concr.* **1983**, *5*, 225–233. [CrossRef]
52. Zhang, X.; Ruiz, G.; Abd Elazim, A. Loading rate effect on crack velocities in steel fiber-reinforced concrete. *Int. J. Impact Eng.* **2015**, *76*, 60–66. [CrossRef]